Journal of Theoretical Biology 484 (2020) 110006

Contents lists available at ScienceDirect

Journal of Theoretical Biology

journal homepage: www.elsevier.com/locate/jtb

Quantification of Predictive Uncertainty in Models of FtsZ ring assembly in *Escherichia coli*

Yanan Ye[a,1], Alvaro Ruiz-Martinez[b,1], Peng Wang[a,c,*], Daniel M. Tartakovsky[d,*]

[a] School of Mathematics and System Sciences, Beihang University, Beijing, China
[b] Department of Mechanical and Aerospace Engineering, University of California, San Diego, La Jolla, CA, USA
[c] Beijing Advanced Innovation Center for Big Data and Brain Computing, Beihang University, Beijing
[d] Department of Energy Resources Engineering, Stanford University, Stanford, CA 94305, USA

ARTICLE INFO

Article history:
Received 24 June 2019
Revised 6 September 2019
Accepted 12 September 2019
Available online 17 September 2019

Keywords:
Uncertainty quantification
FtsZ polymerization
Probability distribution method

ABSTRACT

Quantitative predictions of FtsZ protein polymerization are essential for understanding the self-regulating mechanisms in biochemical systems. Due to structural complexity and parametric uncertainty, existing kinetic models remain incomplete and their predictions error-prone. To address such challenges, we perform probabilistic uncertainty quantification and global sensitivity analysis of the concentrations of various protein species predicted with a recent FtsZ protein polymerization model. Our results yield a ranked list of modeling shortcomings that can be improved in order to develop more accurate predictions and more realistic representations of key mechanisms of such biochemical systems and their response to changes in internal or external conditions. Our conclusions and improvement recommendations can be extended to other kinetics models.

1. Introduction

FtsZ (filamenting temperature-sensitive mutant Z) is a prokaryotic tubulin-like protein conserved in most bacteria. Models of the kinetics of its polymerization further our understanding of the process involved in cell division. Such models are notoriously complex largely due to a large number of protein forms in the polymer assembly process. Many models have been proposed to describe the kinetics of in vivo or in vitro observations of FtsZ assembly. Although many of them are successful in capturing the initial stages of polymerization, some are incapable of handling hydrolysis effects and transformations of filaments and bundles (Ref. Chen and Erickson, 2005), while others (Refs. Lan et al. 2008; Surovtsev et al. 2008; Dow et al. 2013) involve hundreds or thousands of differential equations, solving which might be computationally prohibitively expensive.

Uncertainty associated with model parameters (reaction rate constants) further undermines the utility of such models. Most key parameters exhibit certain levels of heterogeneity in space and time and some cannot be directly measured (Refs. Kennedy and O'Hagan, 2011; Higdon et al., 2004). For instance, the values of bundling dissociation rates were identified as uncertain (Ref. Ruiz-Martinez et al., 2016) and had to be calibrated on related data (Refs. Chen and Erickson, 2005; Chen et al., 2005). Despite continuous improvements in data acquisition technology, measurements of spatiotemporal variations in parameter values remain scarce and prone to measurement errors. Such parametric uncertainty leads to disagreements between experimental observations and computer simulations, and undermines the veracity and, ultimately, utility of model predictions.

We show that rigorous uncertainty quantification and sensitivity analysis can enhance the predictive power of models of FtsZ polymerization and suggest strategies to minimize the predictive error and to reduce predictive uncertainty. To illustrate this approach, we consider the recent kinetics model (Ref. Ruiz-Martinez et al., 2018) because of both its reduced complexity (in terms of a smaller system of ordinary differential equations) and excellent agreement with measurements of the average length and width of the species, the length-to-width ratio, and the concentration of monomers at steady state in a wide range of concentrations (Table 1). Its efficiency, accuracy, and simplicity relative to its counterparts are the main reasons for this modeling choice. Uncertainty in key reaction rate constants is dealt with probabilistically by employing the method of distributions

Abbreviations: PDF, probabilistic density function; MCS, Monte Carlos Simulations; ODE, ordinary differential equations; CV, coefficient of variation; FtsZ, Filamenting temperature-sensitive mutant Z.

* Corresponding author.
E-mail addresses: wang.peng@buaa.edu.cn (P. Wang), tartakovsky@stanford.edu (D.M. Tartakovsky).

[1] Equal effort

https://doi.org/10.1016/j.jtbi.2019.110006
0022-5193/

Table 1
Comparison of the kinetic in vitro models in terms of their complexity, applicability range, and ability to predict the observed features of FtsZ assembly. M1, M2, and M3 designate the single-filament, two-filament-bundling, and multi-filament-bundling models introduced in Ref. Lan et al. (2008), respectively; C_{tot} is the total concentration of FtsZ monomers in all forms; low and high C_{tot} refers to its values of 2 μM and 10 μM, respectively; $C_{\text{cr}}^1 = C_{Z^{\text{na}},\text{ss}} + C_{Z,\text{ss}} \approx 0.7$ μM is the critical concentration at which polymerization begins, it is computed as the sum of the steady-state concentrations of non-activated (GDP-bound) and activated (GTP-bound) FtsZ monomers, respectively; $C_{\text{cr}}^2 \approx 3.0$ μM is the critical value of concentration C_{tot} at which bundling becomes pronounced. The abbreviations "Ave" and "Dist" denote average and distribution, respectively; the superscripts $^+$ and $^-$ denote the overestimated and underestimated predictions, respectively.

Model (reference)	Refs. Chen et al. (2005); Chen and Erickson (2005)	M1 in Ref. Lan et al. (2008)	M2 in Ref. Lan et al. (2008)	M3 in Ref. Lan et al. (2008)	Ref. Surovtsev et al. (2008)	Ref. Ruiz-Martinez et al. (2016)	Ref. Ruiz-Martinez et al. (2018)
Number of ODEs	8	500	500	1254	300	17	10
Short time	Yes	Yes	Yes	Yes	Yes	Yes	Yes
Long time	No	Yes	Yes	Yes	Yes	Yes	Yes
Low C_{tot}	Yes	Yes	Yes	Yes	Yes	Yes	Yes
High C_{tot}	No	No	No	No	Yes	Yes	Yes
Filament length	No	Dist	Dist	Ave$^+$	Dist	Ave	Ave
Bundle width	No	No. 2 filaments	Dist$^+$	No	Dist	Ave	Ave
C_{cr}^1	Yes$^-$	Yes	Yes	Yes	Yes$^-$	Yes	Yes
C_{cr}^2	No	No	No	No	No	Yes	Yes

(Refs. Wang and Tartakovsky, 2012; Wang et al., 2013; Tartakovsky and Gremaud, 2015). The latter has been used in many applications (see, e.g., Refs. Venturi et al., 2013; Alawadhi et al., 2018; Boso and Tartakovsky, 2016; Tartakovsky and Broyda, 2011) to gain both physical insight and computationally efficiency. The probabilistic framework also underpins our global sensitivity analysis, which (unlike its deterministic local counterpart) does not assume that a set of parameters obtained from model calibration is the most likely one – an assumption of questionable validity in complex biochemical models such as that of FtsZ protein polymerization.

2. FtsZ protein polymerization model

The process of FtsZ polymerization involves numerous interactions between monomers, filaments and bundles and is often mathematically represented by systems of ordinary differential equations (ODE) consisting of as many as a thousand of coupled ODEs (Ref. Lan et al., 2008). Solving such large systems is computationally expensive and, more importantly, involves large numbers of uncertain parameters (reaction rate constants). A recently proposed kinetic model (Ref. Ruiz-Martinez et al., 2018) alleviates both of these problems by representing the elongation and bundling processes with just a few steps, which have relatively few parameters. The model consists of ten ODEs,

$$\frac{dC_i}{dt} = g_i(\mathbf{C}), \quad i = 1, \cdots, 10, \tag{1}$$

that describe the temporal evolution of the concentrations $\mathbf{C}(t) = \{C_1, \cdots, C_{10}\} \equiv \{C_{Z^{\text{na}}}, C_Z, C_{Z_2}, C_{Z_3}, C_F, C_{B_2}, C_{B_3}, C_{B_w}, C_{\text{m,fb}}, C_{\text{f,wb}}\}$ of the species denoted by their respective subscripts. Specifically, Z^{na}, Z, Z_2, and Z_3 denote non-activated and activated monomers, dimers and trimers, respectively; B_2 and B_3 represent thin bundles; B_w stands for wide bundles. Finally, $C_{\text{m,fb}}$ and $C_{\text{f,wb}}$ are the concentrations of monomers in long filaments/bundles and filaments in wide bundles, respectively. The functions $g_i(\mathbf{C})$ represent biochemical reactions, such that

$$\begin{aligned}
g_1 &= -k_{\text{ac}}^+ C_1 + k_{\text{ac}}^- C_2 + k_{\text{hy/dis}}^1 C_5 \\
&\quad + k_{\text{hy/dis}}^2 \Sigma_{567} + k_{\text{hy/dis}}^3 \Sigma_{678} \\
g_2 &= k_{\text{ac}}^+ C_1 - k_{\text{ac}}^- C_2 - 2k_{\text{nu}}^+ C_2^2 + 2k_{\text{nu}}^- C_3 \\
&\quad + k_{\text{el}}^- (C_4 + C_5) - k_{\text{el}}^+ C_2 \Sigma_{345} - k_{\text{mb}} C_2 \Sigma_{678} \\
g_3 &= k_{\text{nu}}^+ C_2^2 - k_{\text{nu}}^- C_3 - k_{\text{el}}^+ C_2 C_3 + k_{\text{el}}^- C_4 \\
g_4 &= k_{\text{el}}^+ C_2 (C_3 - C_4) - k_{\text{el}}^- C_4 \\
g_5 &= k_{\text{el}}^+ C_2 C_4 - k_{\text{an}}^+ C_5^2 + k_{\text{an}}^- C_5 - 2k_{\text{bu;(F,F)}}^+ C_5^2 \\
&\quad - k_{\text{bu;(F,B}_2\text{)}}^+ C_5 C_6 - k_{\text{bu;(F,B}_3\text{)}}^+ C_5 C_7 \\
&\quad - k_{\text{bu;(F,B}_w\text{)}}^+ C_5 C_8 + 2k_{\text{bu;B}_2}^- C_6 \\
&\quad + k_{\text{bu;B}_3}^- C_7 + k_{\text{bu;B}_w}^- C_8 + k_{\text{hy/dis}}^2 C_5 \\
g_6 &= k_{\text{bu;B}_3}^- C_7 - k_{\text{bu;B}_2}^- C_6 + k_{\text{bu;(F,F)}}^+ C_5^2 \\
&\quad - k_{\text{bu;(F,B}_2\text{)}}^+ C_5 C_6 + k_{\text{hy/dis}}^2 C_6 \\
g_7 &= -k_{\text{bu;B}_3}^- C_7 + k_{\text{bu;(F,B}_2\text{)}}^+ C_5 C_6 \\
&\quad - k_{\text{bu;(F,B}_3\text{)}}^+ C_5 C_7 + k_{\text{hy/dis}}^2 C_7 \\
g_8 &= k_{\text{bu;(F,B}_3\text{)}}^+ C_5 C_7 - k_{\text{bu;(B}_w\text{,B}_w\text{)}}^+ C_8^2 + k_{\text{bu;B}_w}^- C_8 \\
g_9 &= 4k_{\text{el}}^+ C_2 C_4 + k_{\text{el}}^+ C_2 C_5 - k_{\text{el}}^- C_5 - k_{\text{hy/dis}}^2 \Sigma_{567} \\
&\quad - k_{\text{hy/dis}}^1 C_5 - (k_{\text{hy/dis}}^3 + k_{\text{mb}} C_2) \Sigma_{678} \\
g_{10} &= 4k_{\text{bu;(F,B}_3\text{)}}^+ C_5 C_7 - k_{\text{bu,B}_w}^- C_8 + k_{\text{bu;(F,B}_w\text{)}}^+ C_5 C_8
\end{aligned}$$

where $\Sigma_{klm} \equiv C_k + C_l + C_m$.

Initial concentrations for all species are set to $C_i(t=0) = 0$ for $i = 2, \cdots, 10$ and $C_1(0) = C_{\text{tot}}$, where C_{tot} is the total concentration of FtsZ monomers in all forms (monomer, protofilament, filament, and bundle):

$$\begin{aligned}
C_{\text{tot}} &= \bar{L}_{\text{fb}}^{\text{m}} (C_5 + 2C_6 + 3C_7 + \bar{f}_{\text{wb}} C_8) \\
&\quad + C_1 + C_2 + 2C_3 + 3C_4,
\end{aligned} \tag{2}$$

with $\bar{L}_{\text{fb}}^{\text{m}}$ and $\bar{f}_{\text{wb}}$ denoting the average filament length and the average number of filaments in a wide bundle, respectively. These parameters are expressed in terms of the concentrations as

$$\bar{L}_{\text{fb}}^{\text{m}} = \frac{C_9}{C_5 + 2C_6 + 3C_7 + C_{10}}, \quad \bar{f}_{\text{wb}} = \frac{C_{10}}{C_8}. \tag{3}$$

The average total length and average total number of filaments per bundle are also functions of the concentrations

$$\bar{L}_{\text{tot}}^{\text{m}} = \frac{2C_2 + 3C_3 + C_9}{C_2 + C_3 + C_9/\bar{L}_{\text{fb}}^{\text{m}}}, \tag{4}$$

$$\bar{f}_{\text{tot}} = \frac{2C_2 + 3C_3 + C_9}{2C_2 + 3C_3 + \bar{L}_{\text{fb}}^{\text{m}} (C_5 + C_6 + C_7 + C_8)}. \tag{5}$$

In the rate laws above, k_{ac}^+ and k_{ac}^- are the forward and backward reaction rates of the activation process, respectively; k_{nu}^+ and k_{nu}^- represent the forward and backward reaction rates of the nucleation process, respectively. The forward (k_{el}^+) and backward (k_{el}^-) reaction rates of the elongation process are assumed to be independent of the filament length; and k_{an}^+ and k_{an}^- are the forward and backward reaction rates of the filament annealing process, respectively.

The backward reaction rates k_{el}^{-} and k_{an}^{-} are obtained from the internal energies of filaments and bundles (Ref. Lan et al., 2008) as

$$k_{\mathrm{el}}^{-}=k_{\mathrm{nu}}^{-}\mathrm{e}^{-\Delta U_t},\quad k_{\mathrm{an}}^{-}=k_{\mathrm{nu}}^{-}\mathrm{e}^{-\Delta U_m}, \tag{6}$$

where ΔU_t and ΔU_m denote the increment in the energy of a monomer connected at the end and middle of a filament, respectively. From the conservation of energy, $\Delta U_m=2\Delta U_t$ (Ref. Lan et al., 2008).

The forward and backward reaction rates of the filament bundling, $k_{\mathrm{bu};(R_1,R_2)}^{+}$ and $k_{\mathrm{bu};(R_1,R_2)}^{-}$, are primarily diffusion-limited (Ref. Ruiz-Martinez et al., 2018). Their values depend on the type of the reactants (R_1, R_2) and their product P, $R_1+R_2\rightleftharpoons P$, where R_1, R_2, $P\in\{\mathrm{F},\mathrm{B}_2,\mathrm{B}_3,\mathrm{B}_{\mathrm{w}}\}$. To be specific, the forward bundling rate $k_{\mathrm{bu};(R_1,R_2)}^{+}$ is obtained from the Smoluchowski reaction rate formula for diffusion-limited reactions and the Rouse model diffusion coefficient for short unentangled polymers (Ref. Ruiz-Martinez et al., 2018),

$$k_{\mathrm{bu};(R_1,R_2)}^{+}=\frac{1}{2}\sum_{i=1}^{2}\frac{k_{\mathrm{bu}}^{0+}F_{\mathrm{F}}(\bar{f}_{\mathrm{F}})}{\sqrt[3]{\bar{f}_{R_i}F_{R_i}}}, \tag{7}$$

where k_{bu}^{0+} is the reference association rate, and

$$F_{R_i}=\sum_{k=0}^{7}\frac{a_k}{2^k}\left(\ln\frac{3}{2\bar{f}_{R_i}}\right)^k, \tag{8}$$

with $a_0=1.0304$, $a_1=0.0193$, $a_2=0.06229$, $a_3=0.00476$, $a_4=0.00166$, $a_5=a_6=0$, and $a_7=2.66\times10^{-6}$. In Eq. (7),

$$\bar{f}_{R_i}=\begin{cases}1, & \text{if}\quad R_i=\mathrm{F}\\ 2, & \text{if}\quad R_i=\mathrm{B}_2\\ 3, & \text{if}\quad R_i=\mathrm{B}_3\\ \bar{f}_{\mathrm{wb}}, & \text{if}\quad R_i=\mathrm{B}_{\mathrm{w}}\end{cases} \tag{9}$$

is the average number of filaments in the linear chain molecule R_i, which diffuse and bind laterally to produce a species P; and $F_{R_i}(\bar{f}_{R_i})=F_{\mathrm{F}}(\bar{f}_{\mathrm{F}})$ is calculated according to Eq. (8).

The backward bundling rates $k_{\mathrm{bu};P}^{-}$ is determined from the bond energy per lateral bond U_{b} (Ref. Ruiz-Martinez et al., 2018): For $P=\mathrm{B}_2$,

$$k_{\mathrm{bu};\mathrm{B}_2}^{-}=\begin{cases}k_{\mathrm{bu}}^{0-}, & \bar{L}_{\mathrm{fb}}^{\mathrm{m}}\le 1\\ k_{\mathrm{bu}}^{0-}\mathrm{e}^{-(\bar{L}_{\mathrm{fb}}^{\mathrm{m}}-1)U_b}, & \bar{L}_{\mathrm{fb}}^{\mathrm{m}}>1\end{cases}; \tag{10a}$$

for $P=\mathrm{B}_3$,

$$k_{\mathrm{bu};\mathrm{B}_3}^{-}=\begin{cases}\bar{k}_{\mathrm{bu}}^{0-}\mathrm{e}^{-\Delta U_b}, & \bar{L}_{\mathrm{fb}}^{\mathrm{m}}\le 1\\ k_{\mathrm{bu}}^{0-}\mathrm{e}^{-\bar{L}_{\mathrm{fb}}^{\mathrm{m}}(U_b+\Delta U_b)+U_b}, & \bar{L}_{\mathrm{fb}}^{\mathrm{m}}>1\end{cases}; \tag{10b}$$

for $P=\mathrm{B}_{\mathrm{w}}$, $R_1=\mathrm{F}$ and $R_2=\mathrm{B}_{\mathrm{w}}$,

$$k_{\mathrm{bu};\mathrm{B}_{\mathrm{w}}}^{-}=\begin{cases}0, & \bar{f}_{\mathrm{wb}}\le\alpha_1\\ k_{\mathrm{bu}}^{0-}\mathrm{e}^{-26U_b-27\Delta U_b}, & \bar{f}_{\mathrm{wb}}\in(\alpha_1,\alpha_2)\end{cases} \tag{10c}$$

where $\alpha_1=1.5\times10^{-4}$ and $\alpha_2=1.5\times10^{4}$; and for $P=\mathrm{B}_{\mathrm{w}}$, $R_1=\mathrm{B}_{\mathrm{w}}$ and $R_2=\mathrm{B}_{\mathrm{w}}$,

$$k_{\mathrm{bu};\mathrm{B}_{\mathrm{w}}}^{-}=0. \tag{10d}$$

Here k_{bu}^{0-} is the reference dissociation rate, and ΔU_b represents the incremental bond energy per lateral bond. The experimental studies (Refs. Lan et al., 2008; Dajkovic et al., 2008) found the ratio of incremental longitudinal energy over its lateral counterpart to be $\Delta U_t/\Delta U_b\approx100$.

The dissociation rates of monomers following GTP hydrolysis, $k_{\mathrm{hy/dis}}^{i}$ $(i=1,2,3)$, depend on the polymer concentration:

$$k_{\mathrm{hy/dis}}^{i}=k_{\mathrm{hss/dis}}^{i}\frac{C_{\mathrm{tot}}-C_{Z^{\mathrm{na}}}-C_Z}{C_{\mathrm{tot}}-C_{\mathrm{cr}}^{1}}, \tag{11}$$

where $C_{\mathrm{cr}}^{1}<C_{\mathrm{tot}}$ is the first critical concentration and $k_{\mathrm{hss/dis}}^{1}, k_{\mathrm{hss/dis}}^{2}, k_{\mathrm{hss/dis}}^{3}$ are the steady-state hydrolysis rates for monomers detaching from the end of filaments, from the middle of filaments and thin bundles, and from the thick bundles, respectively. These three rates satisfy the order relation $k_{\mathrm{hss/dis}}^{1}>k_{\mathrm{hss/dis}}^{2}>k_{\mathrm{hss/dis}}^{3}$, since less energy is required to break a longitudinal bond at the filament ends than two bonds at its middle (Ref. Mateos-Gil et al., 2012), whereas the monomers in a bundle can be doubly connected both longitudinally and laterally. Eq. (11) indicates that at the beginning of polymerization, when most FtsZ proteins are in the form of non-activated and activated monomers, i.e., $C_{Z^{\mathrm{na}}}+C_Z\approx C_{\mathrm{tot}}$, the dissociation is almost absent, $k_{\mathrm{hy/dis}}^{i}\approx0$; at steady state, when GDP deactivates monomers with the polymer network is formed, the hydrolysis/dissociation rates reach their maximum values, $k_{\mathrm{hy/dis}}^{i}\approx k_{\mathrm{hss/dis}}^{i}$ with $i=1,2,3$.

Finally, a value of the attachment rate of monomers, k_{mb}, is assumed to be smaller than the forward elongation rate, $k_{\mathrm{mb}}<k_{\mathrm{el}}^{+}$. That is due to the fact that longitudinal attachments of monomers to filament ends are more likely to occur than a mixed longitudinal and lateral attachments in a monomer-bundle interaction.

3. Uncertainty quatification

Exact values of the lateral association rate of filaments, k_{bu}^{0+}, lateral dissociation rate, k_{bu}^{0-}, monomers attachment rate, k_{mb}, and steady-state hydrolysis/dissociation rate, $k_{\mathrm{hss/dis}}^{1}$, are unknown. This parametric uncertainty renders predictions of the concentrations dynamics based on Eq. (1) uncertain as well. Our goal is to quantify this predictive uncertainty probabilistically by treating the four uncertain rate constants as random variables and then obtaining the joint probability density function (PDF) of the ten concentration species $\mathbf{C}(t)$ involved in FtsZ protein polymerization, $f(\mathbf{c};\,t)$, where $\mathbf{c}=(c_1,\ldots,c_{10})$ are possible outcome values of species concentrations $\mathbf{C}(t)$ at any time t. This would allow one to determine, e.g., the probability that concentration of the ith species C_i exceeds a given value c_i $(i=1,\cdots,10)$, $\mathbb{P}[C_i(t)>c_i]$.

We use the method of distributions (Refs. Wang and Tartakovsky, 2012; Wang et al., 2013; Tartakovsky and Gremaud, 2015) to obtain the joint PDF $f(\mathbf{c};\,t)$. The method starts by defining the function

$$\Pi(\mathbf{C},\mathbf{c})\equiv\delta[C_1(t)-c_1]\cdots\delta[C_{10}(t)-c_{10}]. \tag{12}$$

Its ensemble average over realizations of the random vector $\mathbf{C}$, at any time t, equals the joint PDF (Ref. Wang et al., 2013)

$$\mathbb{E}[\Pi]=f(\mathbf{c};t). \tag{13}$$

This result follows directly from the definitions of both the ensemble mean and the Dirac delta function $\delta(\cdot)$. The next step is to derive a ten-dimensional (linear) evolution equation for $\Pi(\mathbf{c},\,t)$ (see the Appendix for details),

$$\frac{\partial\Pi}{\partial t}=-\sum_{i=1}^{10}\frac{[\partial g_i(\mathbf{c})\Pi]}{\partial c_i}, \tag{14}$$

which is subject to the initial condition

$$\Pi(\mathbf{c},0)=\delta(C_{\mathrm{tot}}-c_1)\delta(c_2)\cdots\delta(c_{10}). \tag{15}$$

The functions $g_i(\mathbf{c})$ are first defined in Eq. (1); it is worthwhile emphasizing that random (and unknown) functions $\mathbf{C}(t)$ in $g_i(\mathbf{C})$ in Eq. (1) are now replaced with deterministic (and known) coordinates $\mathbf{c}$.

Table 2
System states and parameters.

Symbol	[unit]	Description	Value
System states			
$C_{Z^{na}}$	[μM]	Concentration of non-activated monomers	–
C_Z	[μM]	Concentration of activated monomers	–
C_{Z_2}	[μM]	Concentration of protofilaments (dimers)	–
C_{Z_3}	[μM]	Concentration of protofilaments (trimers)	–
C_F	[μM]	Concentration of long filaments	–
C_{B_2}	[μM]	Concentration of thin bundles	–
C_{B_3}	[μM]	Concentration of thin bundles	–
C_{B_w}	[μM]	Concentration of wide bundles	–
$C_{m,fb}$	[μM]	Concentration of monomers in long filaments and bundles	–
$C_{f,wb}$	[μM]	Concentration of filaments in wide bundles	–
Model Parameters			
k_{ac}^{+}	[s^{-1}]	Forward activation rate	0.38
k_{ac}^{-}	[s^{-1}]	Backward activation rate	0.01
k_{nu}^{+}	[$\mu M^{-1}s^{-1}$]	Forward nucleation rate	0.79
k_{nu}^{-}	[s^{-1}]	Backward nucleation rate	199.8
k_{el}^{+}	[$\mu M^{-1}s^{-1}$]	Forward elongation rate	6.6
k_{el}^{-}	[$\mu M^{-1}s^{-1}$]	Backward elongation rate	–
k_{an}^{+}	[$\mu M^{-1}s^{-1}$]	Forward filament annealing rate	6.6
k_{an}^{-}	[$\mu M^{-1}s^{-1}$]	Backward filament annealing rate	–
k_{bu}^{+}	[$\mu M^{-1}s^{-1}$]	Forward filament bundling rate	–
k_{bu}^{-}	[s^{-1}]	Backward filament bundling rate	–
$k_{hy/dis}^{1}$	[s^{-1}]	Dissociation rate of non-activated monomers from filaments After GTP hydrolysis	–
$k_{hy/dis}^{2}$	[s^{-1}]	Dissociation rate of non-activated monomers from filaments and bundles after GTP hydrolysis	–
$k_{hy/dis}^{3}$	[s^{-1}]	Dissociation rate of non-activated monomers from bundles after GTP hydrolysis	–
$k_{hss/dis}^{2}$	[s^{-1}]	Dissociation rate of non-activated monomers from filaments and bundles after GTP hydrolysis at the steady state	0.143
$k_{hss/dis}^{3}$	[s^{-1}]	Dissociation rate of non-activated monomers from bundles after GTP hydrolysis at the steady state	0.112
k_{mb}	[$\mu M^{-1}s^{-1}$]	Rate of attachment of monomers to bundles	–
C_{tot}	[μM]	Total concentration of FtsZ monomers in all forms	–
C_{cr}^{1}	[μM]	The first critical concentration	0.7
$\bar{l}_{fb}^{m}$	–	Average filament and bundle length	–
$\bar{f}_{wb}$	–	Number of filaments in a wide bundle	–
$\bar{l}_{tot}^{m}$	–	Average total length	–
$\bar{f}_{tot}$	–	Average number of filaments in a bundle	–
ΔU_t	[k_BT]	Increment energy of a monomer connected at the end of a filament	4.05
ΔU_m	[k_BT]	Increment energy of a monomer connected at the middle of a filament	8.10
U_b	[k_BT]	Bond energy per lateral bond	0.175
ΔU_b	[k_BT]	Increment of lateral energy	0.0405

The initial condition in Eq. (15) reflects our knowledge of the system's initial state: $C_i(t=0)=0$ for $i=2,\cdots,10$ and $C_1(0)=C_{tot}$. If C_{tot} is uncertain and described probabilistically in terms of its PDF $f_{C_{tot}}(c_{tot})$, then the ensemble average of Eq. (15) yields the initial condition for the joint PDF, $f(\mathbf{c},0)=f_{C_{tot}}(c_1)\delta(c_2)\cdots\delta(c_{10})$. If the value of C_{tot} is known with certainty, as is the case in the simulations reported below, then its PDF is $f_{C_{tot}}(c_{tot})=\delta(C_{tot}-c_{tot})$ and the initial condition for the joint PDF reduces to $f(\mathbf{c},0)=\delta(C_{tot}-c_1)\delta(c_2)\cdots\delta(c_{10})$.

The functions $g_i(\mathbf{c})$ are parameterized by a large number of the reaction rate constants introduced in the previous section. All but four of those are known with a reasonable degree of certainty. Their values are collated in Table 2; they are taken from in vitro studies of FtsZ-F268C polymerization (Refs. Chen and Erickson, 2005; Arumugam et al., 2014; Lan et al., 2008; Dajkovic et al., 2008). The initial condition C_{tot} is set to 1.0 μM and the first critical concentration $C_{cr}^{1}=0.7\mu M$ (Ref. Chen and Erickson, 2005).

Statistics of the four random rate constants, k_{bu}^{0+}, k_{bu}^{0-}, k_{mb} and $k_{hss/dis}^{1}$, in Table 3 are inferred from both past investigations (Refs. Chen and Erickson, 2005; Arumugam et al., 2014; Lan et al., 2008; Dajkovic et al., 2008; Ruiz-Martinez et al., 2018) and the parametric constraints discussed in the previous section. The first three parameters are reported in the literature with finite ranges, $k_{bu}^{0+}\in[2.0,7.5]$, $k_{bu}^{0-}\in[0,500]$ and $k_{mb}\in[2.0,6.6]$; we model them as Gaussian variables, whose means are taken as the past guesses and variances are one-sixth of their respective intervals. The upper bound of $k_{hss/dis}^{1}$ is not available, $k_{hss/dis}^{1}\geq 0.143$; hence, we treat it as a log-normal random variable, whose mean is the logarithm of the past guess ($\ln 0.7$) and variance is one-third of the distance between the median value and the low bound.

Table 3
Statistical properties of the uncertain (random) reaction rate constants.

Parameter	k_{bu}^{0+}	k_{bu}^{0-}	k_{mb}	$k_{hss/dis}^{1}$
Probabilistic Distribution	Normal	Normal	Normal	Log-Normal
Mean	4.75	250	4.1	−0.3567
Variance	0.9167	83.33	0.7	0.6483

We use Monte Carlo simulations (MCS) to solve the "raw" PDF Eq. (14): for each of the $N_{MCS}=5000$ realizations of the four random rate constants, $\{k_{bu}^{0+},k_{bu}^{0-},k_{mb},k_{hss/dis}^{1}\}_n$ with $n=1,\cdots,N_{MCS}$, Eqs. (14) and (15) are solved numerically (see the Appendix for details) to obtain the corresponding solution $\Pi_n(\mathbf{c},t)$. The relationship (13) between the ensemble mean of Π and the joint PDF $f(\mathbf{c};t)$ implies that

$$f(\mathbf{c};t)\approx\frac{1}{N_{MCS}}\sum_{n=1}^{N_{MCS}}\Pi_n(\mathbf{c},t). \tag{16}$$

This strategy for computing the joint CDF $f(\mathbf{c};t)$ is considerably more efficient than the use of MCS to solve the original problem (1). That is because orders of magnitude more MC

Table 4
Statistical information of species concentrations at their steady states.

	1 μM			3 μM		
	Mean	Variance	Coefficient of variation	Mean	Variance	Coefficient of variation
$C_{Z^{na}}$	0.1085	0.0011	0.3121	0.1674	0.0240	0.9242
C_Z	0.6009	0.0018	0.0706	0.4794	0.0086	0.1939
C_{Z_2}	0.0014	3.18×10^{-8}	0.1256	0.0009	1.35×10^{-7}	0.3924
C_{Z_3}	0.0008	1.31×10^{-8}	0.1511	0.0005	5.32×10^{-8}	0.5038
C_F	0.0414	4.99×10^{-6}	0.0539	0.0494	8.89×10^{-6}	0.0604
C_{B_2}	0.0120	0.1049	27.023	0.0682	1.2476	16.366
C_{B_3}	0.0085	0.0535	27.258	0.0496	0.7383	17.321
C_{B_w}	0.0017	2.75×10^{-5}	3.0848	0.0466	0.0001	0.2512
$C_{m,fb}$	0.2855	0.0035	0.2079	2.3500	0.0335	0.0779
$C_{f,wb}$	0.0001	2.66×10^{-5}	33.440	0.0021	7.73×10^{-5}	4.1541
$\bar{L}^m_{tot}$	6.7131	1.6823	0.1932	29.243	6.2784	0.0857
$\bar{f}_{tot}$	0.9476	0.0746	0.2882	0.7449	0.0197	0.1883
$\bar{L}^m_{tot}/\bar{f}_{tot}$	7.4917	7.7266	0.3710	40.651	75.647	0.2140

realizations are needed to estimate a solution's PDF than a solution's mean with the same accuracy. The former is needed when solving Eq. (1), while the latter is sufficient when solving Eq. (14).

4. Sensitivity analysis

The probabilistic treatment of the set of four reaction rate constants $\mathcal{A} = \{k^{0+}_{bu}, k^{0-}_{bu}, k_{mb}, k^1_{hss/dis}\}$ facilitates global sensitivity analysis, which is based on ANOVA (analysis of variance). Specifically, we employ a Sobol index called the total sensitivity $\mathcal{S}_{i,j}$ of the ith species concentration C_i $(i = 1, \cdots, 10)$ to uncertainty in the jth rate constant $(j = 1, \cdots, 4)$ from the set $\mathcal{A}$. It is estimated from N_{NMC} solves of Eq. (1), parameterized with realizations $\mathcal{A}_n$ and $\mathcal{A}^j_n$ $(n = 1, \cdots, N_{NMC})$, as

$$\mathcal{S}_{i,j} = \frac{1}{2N_{NMC}\sigma^2_{C_i}} \sum_{n=1}^{N_{NMC}} \left[C_i(\mathcal{A}_n) - C_i(\mathcal{A}^j_n)\right]^2, \tag{17}$$

where $\sigma^2_{C_i}$ is the variance of C_i, and $C_i(\mathcal{A}_n)$ and $C_i(\mathcal{A}^j_n)$ refer to the solutions computed with $\mathcal{A}_n$ and $\mathcal{A}^j_n$, respectively. The reaction rate sets $\mathcal{A}_n$ and $\mathcal{A}^j_n$ differ in the j-th reaction rates. (For example, if $N_{NMC} = 2$, and $\mathcal{A}_1 = (1, 2, 3, 4)$ and $\mathcal{A}_2 = (5, 6, 7, 8)$, then $\mathcal{S}_{i,1} \sim \sum_{n=1}^{2}[C_i(\mathcal{A}_n) - C_i(\mathcal{A}^1_n)]^2 = [C_i(1, 2, 3, 4) - C_i(5, 2, 3, 4)]^2 + [C_i(5, 6, 7, 8) - C_i(1, 6, 7, 8)]^2$.)

A small value of $\mathcal{S}_{i,j}$ suggests that a value of the j-th reaction rate is unimportant to the i-th species concentration.

5. Results and discussion

5.1. Uncertainty quantification

When quantified probabilistically, uncertainty in values of the reaction rate constants k^{0+}_{bu}, k^{0-}_{bu}, k_{mb} and $k^1_{hss/dis}$ propagates through the modeling process, giving rise to uncertain (probabilistic) predictions of the reacting species in Eq. (1). These take form of the marginal PDFs, whose temporal snapshots are displayed in Figs. 1–5 at time t ranging from 0 to 30 s. PDFs of individual species, $f_{C_i}(c_i; t)$ with $i = 1, \cdots, 10$, are computed as marginals of the joint PDF $f(\mathbf{c}; t)$.

At initial time $(t = 0)$, the PDFs are represented by vertical lines, reflecting the assumed certainty in the initial state. Uncertainty in predictions of all species concentrations increases, as evidenced by the widening of their PDFs. Nearly all species exhibit highly asymmetric (non-Gaussian) PDFs, which limits the utility of standard deviation or variance as a measure of predictive uncertainty. The concentration PDFs of non-activated ($C_{Z^{na}}$) and activated monomers (C_Z), dimers (C_{Z_2}), trimers (C_{Z_3}), filaments (C_F) and monomers in long filaments and bundles ($C_{m,fb}$) change considerably with time until reaching their steady states at $t = 30$ s. This is in contrast to the concentration PDFs of thin bundles (C_{B_2} and C_{B_3}), wide bundles (C_{B_w}) and filaments in wide bundles ($C_{f,wb}$), all of which remain close to their initial states but with increasingly long tails (shown in the embedded plots).

Table 4 collates the means (μ_i), variances (σ^2_i) and coefficients of variation ($CV = \sigma_i/\mu_i$) of all ten species ($i = 1, \cdots, 10$) at $t =$ 30 s (steady state). As one might have expected, predictions of most of the species with lowest concentrations are subject to the largest uncertainty. For example, predictions of the concentrations of thin bundles (C_{B_2} and C_{B_3}) and filaments in wide bundles ($C_{f,wb}$) have double-digit CVs. For these quantities, it is preferable to look at exceedance probability, which is readily computable from the PDFs, but cannot be ascertained from CV. Although not shown here, we found that beyond $t = 30$ s, CVs of $C_{Z^{na}}$, C_Z, C_{Z_2}, C_{Z_3}, C_F and $C_{m,fb}$, remain relatively constant.

Uncertainty in k^{0+}_{bu}, k^{0-}_{bu}, k_{mb} and $k^1_{hss/dis}$ has no discernible impact on the model's ability to predict some of the key biological features at steady state. For example, the PDF of the concentration of filament species, C_F, remains narrow for a range of the total concentration ($C_{tot} = 1$ μM and 3 μM). This finding is unexpected since the filament production is directly related to the (uncertain) backward bundling rate, k^{0-}_{bu}. Uncertainty in the dissociation rate after hydrolysis, $k^1_{hss/dis}$, does not induce appreciable uncertainty in predictions of the concentration of non-activated monomers, $C_{Z^{na}}$; and uncertainty in the attachment rate of monomers to bundles, k_{mb}, does not significantly impact uncertainty in predictions of the concentration of activated monomers, C_Z. At $C_{tot} = 1$ μM, only uncertainty in predictions of the concentration of wide bundles, C_{B_w}, is significant because the production and consumption of that species are highly dependent on the uncertain forward bundling rate, k^{0+}_{bu}. These findings indicate the robustness of model predictions to inevitable uncertainty in the key model parameters.

Uncertainty in the reaction rates' values does affect uncertainty in predictions of the steady-state bundling steps (C_{B_2}, C_{B_3}, $C_{f,wb}$). That is because the bundling and hydrolysis rates depend on the approximated average features of the species (Eqs. (7)–(11)) which, in turn, depend on the species concentrations (Eq. (3)). Consequently, the predictive uncertainty propagates from the average features to the rest of the species as the total concentration, C_{tot}, increases. Thus, the CVs of small species and filaments are larger at $C_{tot} = 3$ μM than at $C_{tot} = 1$ μM (Table 4).

Predictive robustness of the key steady-state features described by Eqs. (3)–(5) stems from the balance between the concentrations of three general categories: small species, filaments, and bundles. The CVs of the concentrations of monomers and short

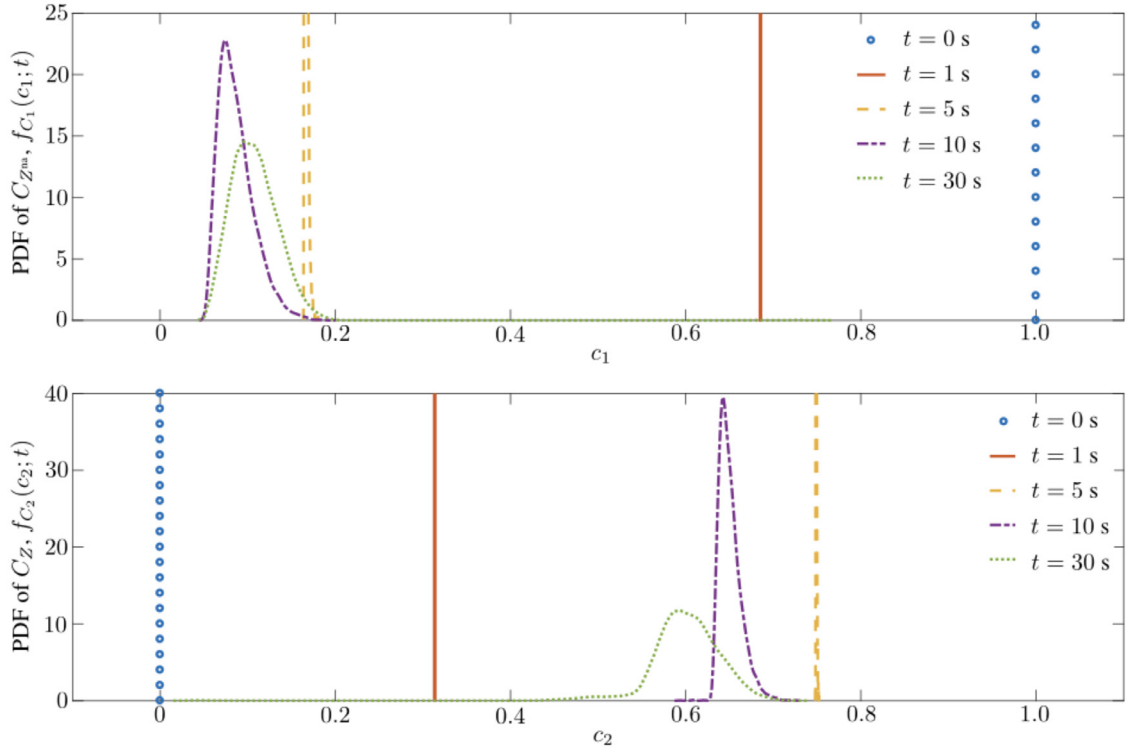

Fig. 1. Temporal evolution of the marginal PDFs of $C_{Z^{na}}$ and C_Z from initial time ($t = 0$) until steady state ($t = 30$ s).

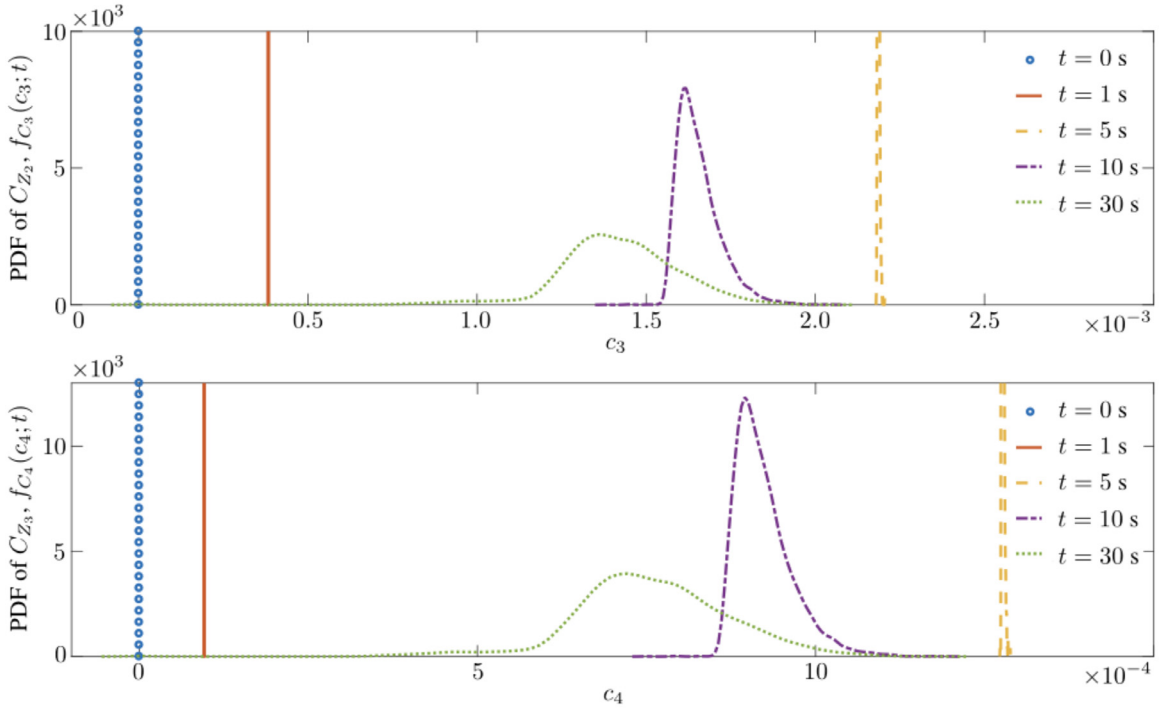

Fig. 2. Temporal evolution of the marginal PDFs of C_{Z_2} and C_{Z_3} from initial time ($t = 0$) until steady state ($t = 30$ s).

filaments, $C_{Z^{na}}$, C_Z C_{Z_2}, and C_{Z_3}, increase with C_{tot}, while predictive uncertainty in the concentrations of bundles, C_{B_2}, C_{B_3}, C_{B_w}, and $C_{f,wb}$, decreases. Predictive uncertainty for the intermediate category, i.e., the concentration of filaments, C_F, is insensitive to the total concentration. This balance affects the predictive uncertainty for our quantities of interest in Eqs. (3)–(5) as follows.

Predictive uncertainty (CV) for the *average total length*, $\bar{L}^{m}_{tot}$, which depends on all of the above concentrations, is low and decreases as C_{tot} increases. The steady-state concentrations of filaments or bundles can vary as long as the average length of the species retains its robust representative value. Such a phenomenon has been observed experimentally at concentrations equal to or larger than $C_{tot} = 3$ μM; it is critical for the robustness of the

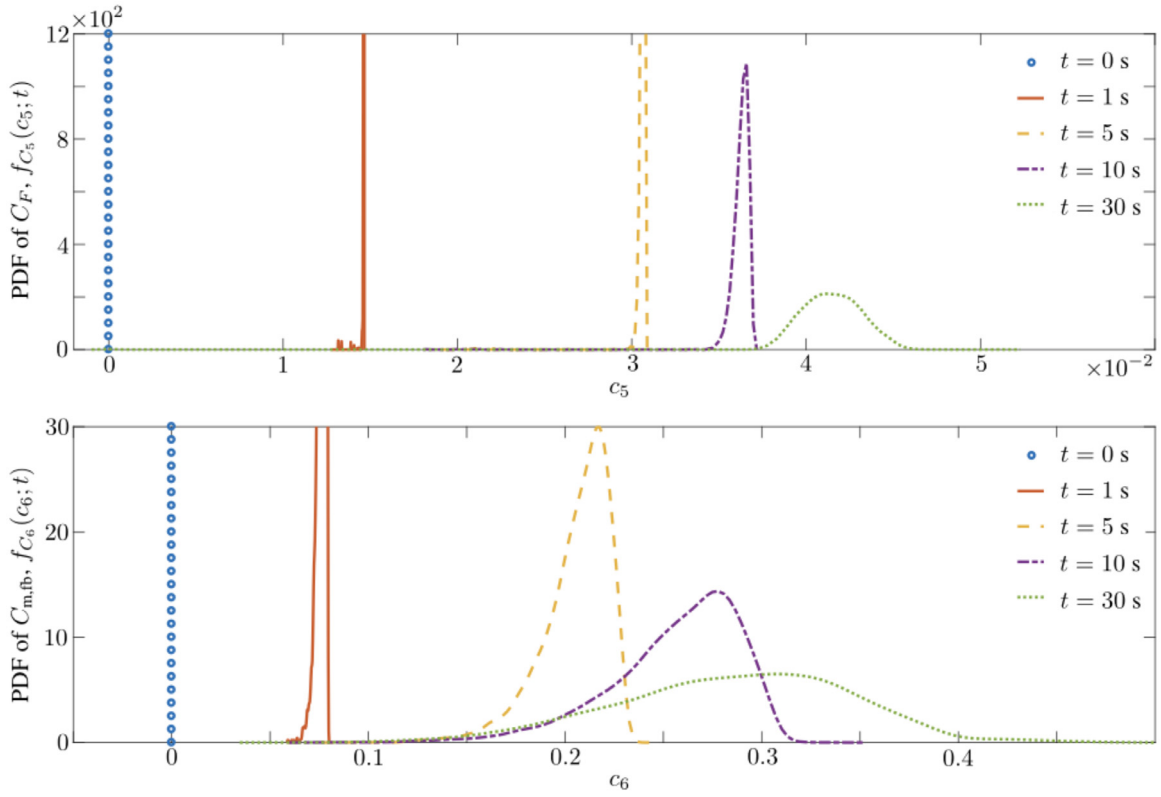

Fig. 3. Temporal evolution of the marginal PDFs of C_F and $C_{\mathrm{m,fb}}$ from initial time ($t = 0$) until steady state ($t = 30$ s).

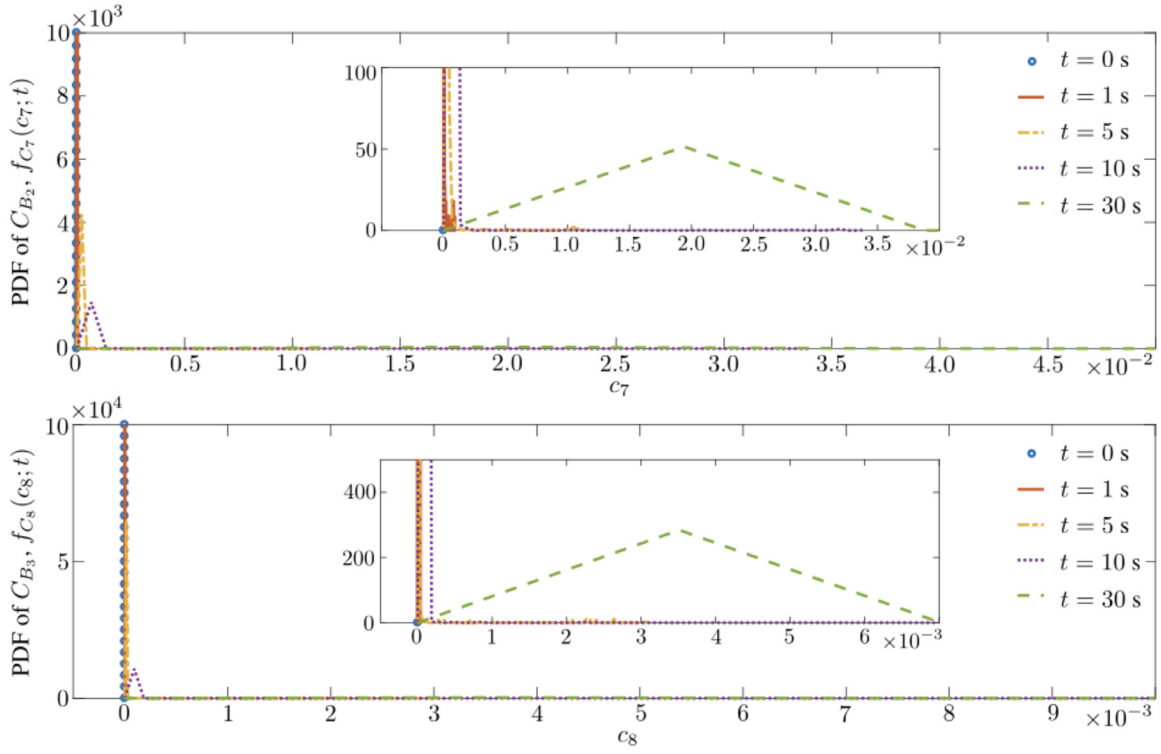

Fig. 4. Temporal evolution of the marginal PDFs of C_{B_2} and C_{B_3} from initial time ($t = 0$) until steady state ($t = 30$ s).

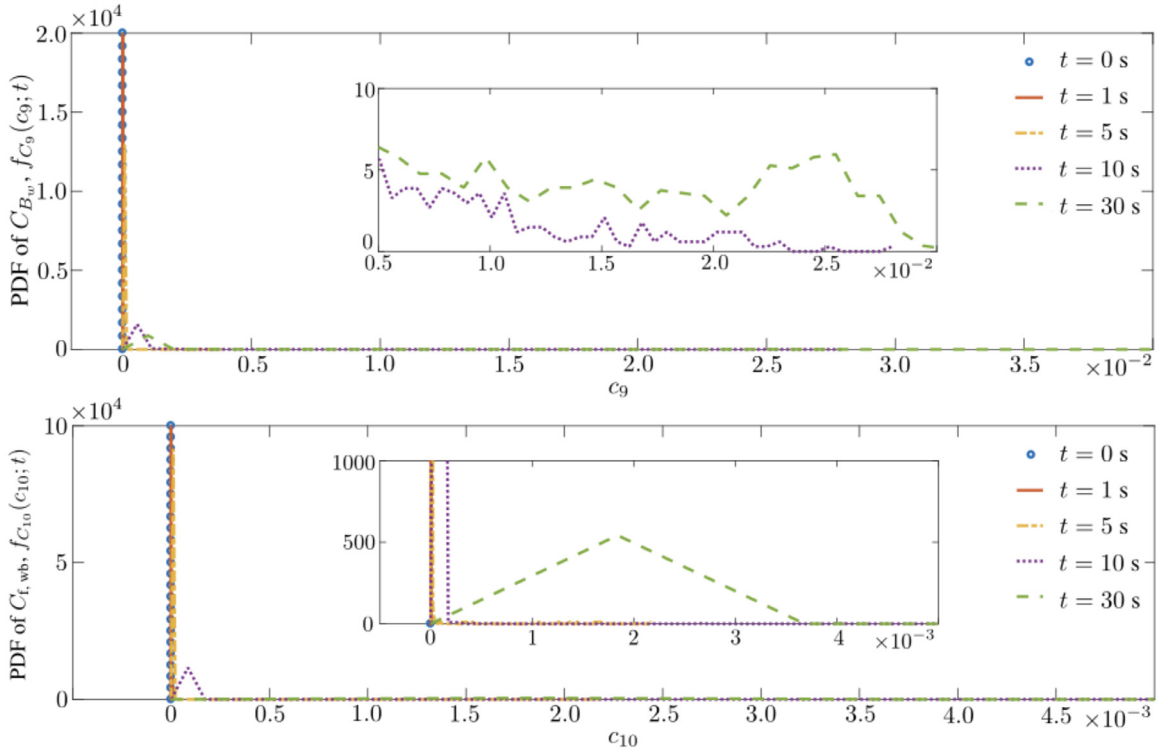

Fig. 5. Temporal evolution of the marginal PDFs of C_{B_w} and $C_{\mathrm{f,wb}}$ from initial time ($t = 0$) until steady state ($t = 30$ s).

polymer network (Refs. Chen et al., 2005; Dajkovic et al., 2008; Huecas et al., 2008; Erickson et al., 2010).

Predictive uncertainty (CV) for the *average total number of filaments per bundle*, $\bar{f}_{\mathrm{tot}}$, is low but somewhat higher than that for $\bar{L}^{\mathrm{m}}_{\mathrm{tot}}$. The predicted values of $\bar{f}_{\mathrm{tot}}$ are robust (around 1) for $C_{\mathrm{tot}} = 1 - 3$ μM because bundles are present but not predominant in that range of C_{tot} (Refs. Chen et al., 2005; Chen and Erickson, 2005; Dajkovic et al., 2008; Huecas et al., 2008; Romberg et al., 2001).

Predictive uncertainty (CV) for the *concentration of monomers* in filaments and bundle form, $C_{\mathrm{m,fb}}$, is low and does not change with the total concentration, C_{tot}. It means that the sum of the species in monomer form, $C_{Z^{\mathrm{na}}} + C_Z$, remains constant at different total concentrations. This physical phenomenon guarantees the stability of the polymer network observed in both in vitro and in vivo experiments at steady state; it is properly captured by many polymerization models (Refs. Romberg and Mitchison, 2004; Chen and Erickson, 2005; Lan et al., 2008; Surovtsev et al., 2008).

The preceding analysis deals with the parametric uncertainty in a given model of FtsZ polymerization [Ref. Ruiz-Martinez et al. (2018)]. It can be augmented with an analysis of structural (model) uncertainty, which could be reduced by the following model improvements at the cost of increased computational cost.

1. Increase the representational accuracy of the bundling reaction rates. Models with fewer species and reactions generally introduce more complexity and variability in the reaction rates. For example, the proposed reduction in the numbers of species and reactions in Ref. Ruiz-Martinez et al. (2018) relative to those in Ref. Ruiz-Martinez et al. (2016) increased dependence of the bundling rates on the average size of bundles.
2. Introduce a few more intermediate bundling steps until a wide bundle species, B_{w}, is reached, while maintaining an efficient accuracy/computational cost balance. This amounts to an increase in the number of species, B_4, B_5, etc., and their corresponding reaction rates and ODEs.
3. Include the GDP and GTP nucleotide species that activate and deactivate FtsZ monomers. That would provide a more detailed description of the monomer dissociation mechanism upon hydrolysis.
4. The experimental observations taken as reference to develop the in vitro model in Ref. Ruiz-Martinez et al. (2018) and other recent kinetics models (Refs. Chen and Erickson, 2005; Lan et al., 2008; Surovtsev et al., 2008; Ruiz-Martinez et al., 2016) are reported only for thin bundles. Including information from cases with the presence of wider bundles would reduce predictive uncertainty for concentrations of the big species.

5.2. Sensitivity analysis

We supplement our uncertainty quantification study with a global sensitivity analysis, which aims to characterize the impact of variability in the reaction rate constants k^{0+}_{bu}, k^{0-}_{bu}, k_{mb} and $k^{1}_{\mathrm{hss/dis}}$ on the variability in the model predictions of the key quantities of interest (the average length and width of the species, the length-to-width ratio, and the concentration of monomers). These quantities guarantee the robustness and stability of the FtsZ network at steady state, and have been the focus of previous investigations (Refs. Chen et al., 2005; Chen and Erickson, 2005; Lan et al., 2008; Surovtsev et al., 2008; Chen and Erickson, 2009). The results of our sensitivity analysis are reported in Table 5, which lists the total sensitivity of each quantity of interest at steady state ($t = 30$ s) for two total concentrations, $C_{\mathrm{tot}} = 1$ and 3 μM.

Sensitivity to $k^{1}_{\mathrm{hss/dis}}$: We find the dissociation rate of monomers from filament ends after hydrolysis $k^{1}_{\mathrm{hss/dis}}$ to significantly impact the species of the first steps of polymerization and the geometrical features at $C_{\mathrm{tot}} = 1$ μM. This impact is substantially reduced at $C_{\mathrm{tot}} = 3$ μM for the filament species and the average geometrical features because $k^{1}_{\mathrm{hss/dis}}$ is associated with the exchange of monomers between the pool of monomers and filaments at low concentrations (Refs. Chen et al., 2005; Chen and Erickson, 2005). When polymers are mostly single-stranded and not too

Table 5
Sensitivities of $k^1_{\mathrm{hss/dis}}$, k_{mb}, k^{0+}_{bu} and k^{0-}_{bu} at steady state (30 s). S^{tot} is total sensitivity index.

	1 μM					3 μM				
S^{tot}	$k^1_{\mathrm{hss/dis}}$	k_{mb}	k^{0+}_{bu}	k^{0-}_{bu}	Total	$k^1_{\mathrm{hss/dis}}$	k_{mb}	k^{0+}_{bu}	k^{0-}_{bu}	Total
$C_{Z^{\mathrm{na}}}$	0.7852	0.0003	0.0166	0.2026	1.0047	0.7170	0.0004	0.0036	0.2285	0.9495
C_Z	0.6843	0.0067	0.1778	0.3590	1.2278	0.4748	0.0592	0.1353	0.4730	1.1423
C_{Z_2}	0.7600	0.0052	0.1668	0.2737	1.2057	0.5621	0.0491	0.1342	0.3965	1.1419
C_{Z_3}	0.7822	0.0045	0.1568	0.2460	1.1895	0.5930	0.0448	0.1325	0.3754	1.1457
C_F	0.7859	0.0006	0.0058	0.2378	1.0301	0.0790	0.0031	0.0400	0.9270	1.0491
C_{B_2}	4.77×10^{-6}	2.43×10^{-8}	2.94×10^{-6}	0.7193	0.7193	0.0006	0.0023	0.0002	0.9906	0.9937
C_{B_3}	3.49×10^{-8}	3.74×10^{-11}	1.09×10^{-8}	0.7914	0.7914	0.0003	0.0001	0.0026	1.0079	1.0109
C_{B_w}	0.1531	3.82×10^{-5}	0.6397	0.9337	1.7265	0.2107	0.0042	0.3847	0.7926	1.3922
$C_{\mathrm{m,fb}}$	0.9429	0.0022	0.0507	0.0734	1.0692	0.8612	0.0231	0.0439	0.1313	1.0595
$C_{\mathrm{f,wb}}$	0.0021	1.57×10^{-6}	0.0037	2.9544	2.9602	0.0056	0.0028	0.0626	0.9815	1.0525
$\bar{L}^{\mathrm{m}}_{\mathrm{tot}}$	0.8592	0.0018	0.0697	0.1219	1.0526	0.0660	0.0035	0.0862	0.8315	0.9871
$\bar{f}_{\mathrm{tot}}$	0.8776	0.0003	0.1066	0.1673	1.1518	0.1208	0.0018	0.0638	0.8075	0.9939
$\bar{L}^{\mathrm{m}}_{\mathrm{tot}}/\bar{f}_{\mathrm{tot}}$	0.7159	0.0032	0.2283	0.2613	1.2087	0.2606	0.0055	0.1231	0.6816	1.0709

long, i.e., at $C_{\mathrm{tot}} < 3$ μM, the dominant detachment of monomers after hydrolysis occurs at the ends of filaments. Only when filaments are long enough for bundles to become relevant, i.e., for $C_{\mathrm{tot}} > 3$ μM, the impact of two other types of monomer dissociation rates after hydrolysis, $k^2_{\mathrm{hss/dis}}$ and $k^3_{\mathrm{hss/dis}}$, becomes dominant (Ref. Arumugam et al., 2014). We also observe that the concentration of wide bundles, $C_{\mathrm{B_w}}$, is slightly sensitive to changes in $k^1_{\mathrm{hss/dis}}$. That is due to the high correlation between the rate constants, whose sum of Sobol indices exceeds 1.

Sensitivity to k_{mb}: Although the exchange of monomers between the pool of monomers and the rest of the species is critical for polymer network stability (Refs. Chen et al., 2005; Chen and Erickson, 2005; Koskinen and Hotulainen, 2014; Medeiros et al., 2006), none of the species concentrations and features is sensitive to the attachment rate of monomers to bundles, k_{mb}. Monomers are more likely to attach laterally to bundles than to filaments, partly because there are more lateral binding sites. Previous studies (Refs. Dajkovic et al., 2008; Lan et al., 2008) determined a weaker (about 100 times) strength of the lateral bonds than longitudinal bonds. The apparent insensitivity to k_{mb} is directly related to this property. On the other hand, as C_{tot} increases, the concentrations and features become more sensitive to this rate. It is due to the increase in the number of monomers attaching to the filament ends (Ref. Du et al., 2018); in this case, the number of filaments and fragments of filaments that conform the bundles (Ref. Arumugam et al., 2014).

Sensitivity to k^{0+}_{bu}: The forward bundling rate k^{0+}_{bu} has a considerable impact on the concentrations of activated monomers (C_Z), dimers (C_{Z_2}), trimers (C_{Z_3}) and wide bundles ($C_{\mathrm{B_w}}$). Among them, $C_{\mathrm{B_w}}$ is most sensitive to changes in k^{0+}_{bu}. These findings are to be expected from the kinetic model in Eq. (1), wherein the forward bundling rates primarily regulate the dynamics of wide bundles. The low sensitivity of the geometrical features and the concentration of monomers to changes in k^{0+}_{bu} rate reflects the robustness and stability of the polymer network (Refs. Dajkovic et al., 2008; Huecas et al., 2008; Romberg et al., 2001; Erickson et al., 2010).

Sensitivity to k^{0-}_{bu}: All species concentrations and features are sensitive to the backward bundling rate k^{0-}_{bu}, except those of the monomers in filaments and bundle form, $C_{\mathrm{m,fb}}$. Such high sensitivities are due to the close relation between longitudinal and lateral growth. The backward nucleation rate (or longitudinal detachment of two monomers) (Refs. Chen et al., 2005; Chen and Erickson, 2005) and the backward bundling rate (or lateral detachment of two monomers) have similar values ($\sim 200\ \mathrm{s}^{-1}$) (Refs. Ruiz-Martinez et al., 2016; Ruiz-Martinez et al., 2018). Changes in one of those rates break the polymer growth balance; consequently, both the concentration and size of all species are notably altered. Earlier studies (Refs. Chen et al., 2005; Lan et al., 2008; Ruiz-Martinez et al., 2016) showed the fast rate of both longitudinal and lateral detachment and the importance of such a balance in determining the second critical concentration, which defines the transition from the dominant longitudinal growth stage to the dominant lateral growth stage.

Finally, we examine cross-correlations between the reaction rate constants, k^{0+}_{bu}, k^{0-}_{bu}, k_{mb} and $k^1_{\mathrm{hss/dis}}$, and the role of bundling in the turnover of monomers. If Sobol indices $\mathcal{S}_{i,j}$ for the ith species concentration with respect to the jth rate constant from the set of four, $\mathcal{A}$, are such that $\sum_{j=1}^{4} \mathcal{S}_{i,j} > 1$, then there is a potential correlation between the reaction rates. Table 5 shows that the sums of Sobol indices for C_Z, C_{Z_2}, C_{Z_3} (the smallest species), $C_{\mathrm{B_w}}$, $C_{\mathrm{f,wb}}$ (the largest species), and polymer features are considerably larger than or close to one. Since the four reaction rates are related to both attachment/detachment of monomers ($k^1_{\mathrm{hss/dis}}$ and k_{mb}) and formation of bundles (k^{0+}_{bu} and k^{0-}_{bu}), we posit that there is a strong dependence between the concentrations and rates related to monomers' turnover and bundling processes. Past studies (Refs. Chen et al., 2005; Koskinen and Hotulainen, 2014; Medeiros et al., 2006) showed the relevance of monomer exchanges between the pool and large-size species and their role in network stability. In both in vitro and in vivo scenarios, for any total concentration C_{tot} larger than the first critical concentration (0.7 μM), bundling process governs the turnover of monomers to: i) maintain a constant GTP-hydrolysis/dissociation rate, ii) regulate the average length of the species, and iii) keep the polymer network in equilibrium (Refs. Chen and Erickson, 2005; Ruiz-Martinez et al., 2016; Ruiz-Martinez et al., 2018).

Our results also show that the cross-correlations between the four reaction rates diminish as the total concentration C_{tot} decreases. The presence of bundles at steady state with large C_{tot} and their dominant influence on the dissociation of monomers after hydrolysis have been observed and studied in both in vitro and in vivo (Refs. Romberg et al., 2001; Romberg and Mitchison, 2004; Dajkovic et al., 2008; Huecas et al., 2008; Erickson et al., 2010; Arumugam et al., 2014). It is an essential and natural mechanism in FtsZ assembly kinetics to guarantee a constant monomer exchange rate between the polymer network and the pool. In such regimes, the post-hydrolysis dissociation rate of monomers to short filaments, $k^1_{\mathrm{hss/dis}}$, is not as relevant as the rates related to bigger species, $k^2_{\mathrm{hss/dis}}$ and $k^3_{\mathrm{hss/dis}}$ (for thin (Ref. Chen and Erickson, 2005) and wide (Ref. Arumugam et al., 2014) bundles, respectively). This reduces the correlation between $k^1_{\mathrm{hss/dis}}$ and the rest of the four uncertain parameters.

Combining our results with those from Refs. Ruiz-Martinez et al., 2016; Ruiz-Martinez et al., 2018 allows us to compare the

relative importance of multiple reactions involved in the turnover of monomers:

Attachment of monomers to larger species: Addition of activated monomers to filaments is important in all regimes (i.e., at short and long times as well as at low and high total concentrations). This study shows that attachment of activated monomers to bundles is much less relevant than their attachment to filament ends when bundles are not predominant. As the concentration of big species increases, the interaction of monomers and bundle ends becomes significant (Refs. Romberg et al., 2001; Romberg and Mitchison, 2004; Arumugam et al., 2014).

Detachment of monomers from larger species: Likewise, detachment of activated monomers from filaments is important in all regimes (at short and long times as well as at low and high total concentrations). Detachment of non-activated monomers from filament ends after hydrolysis is mostly dominant when filaments are short, i.e., at short times and/or low concentrations. Recent experimental observations [Ref. Du et al. (2018)] show that the dissociation of monomers from the middle of filaments after GTP hydrolysis reaction can be neglected. Such behavior is predicted in Ref. Ruiz-Martinez et al. (2018) when that reaction is neglected, i.e., the same results are obtained regardless of whether or not such reaction is included in the model. In the case of bundles, however, monomers detach from their filament ends due to treadmilling/hydrolysis (as observed in *in vitro* experiments in Ref. Arumugam et al. (2014)), sometimes causing breakage of partially connected bundles. That is equivalent to the dissociation of monomers from thin bundles after GTP hydrolysis reaction, a process included in terms of their average values in Refs. Ruiz-Martinez et al. (2016, 2018). We conclude that detachment of non-activated monomers from the ends of bundles composed of fragmented filaments after hydrolysis is an essential process which determines the properties of the species and the stability of the system at steady state.

6. Summary and conclusions

We conducted rigorous uncertainty quantification and sensitivity analysis to establish the predictive power of FtsZ protein polymerization models. The latter are a central component of biopolymer network models. While many of the reaction rate constants in such models are well constrained by data, values of the four rates are highly uncertain. These are lateral association rate of filaments, lateral dissociation rate, monomers attachment rate and the steady-state hydrolysis/dissociation rate. We treated these uncertain rate constants as random variables and employed the method of distributions to quantify the impact of parametric uncertainty on probabilistic predictions of the concentrations of species involved in the polymerization process. Our approach enables one to identify experimental strategies for reducing uncertainty in predictions of species concentration and to select a proper model complexity consistent with the quantity and quality of available data.

Our global sensitivity analysis is instrumental in determining the relative importance of attachment/detachment of species to network stability. For example, we found lateral/longitudinal binding/unbinding mechanisms to play a critical role in processes such as elongation/bundling balance or detachment of monomers after hydrolysis. Our results also corroborate certain physiological insights obtained in earlier studies (Refs. Koskinen and Hotulainen, 2014; Medeiros et al., 2006; Huecas et al., 2008; Arumugam et al., 2014).

The reaction rates analyzed in this study are mainly related to the bundling and turnover of monomers. Since those processes were observed in other cytoskeletal biopolymers, we posit that our analysis and conclusions can be extended and generalized to other polymerization kinetics models. The presence of bundles is common in network assembly of actin (fimbrin or α-actinin), microtubules (MAP2) and intermediate filaments (MreB and ParM) (Refs. Falzone et al., 2012; Masuda et al., 2012; Alberts et al., 2014). Similarly to FtsZ polymerization/depolymerization by the action of GTP/GDP nucleotides, the presence of ATP/ADP keeps a permanent balance of the amount of attached/detached monomers to/from actin filaments (Refs. Needleman, 2015; Swanson and Wingreen, 2011; Wegner, 1976).

Declaration of Competing Interest

The authors declare that they have no conflicts of interest with the contents of this article.

Acknowledgments

P. Wang and Y. Ye were partially funded by the National Natural Science Foundation of China (Grant No. 11571028) and the National Key Research and Development Program of China (Grant No. 2017YFB0701700).

Appendix A. Derivation of raw PDF equation

We define $\delta_i \equiv \delta[C_i(t) - c_i]$, which enables us to rewrite Eq. (12) as $\Pi(\mathbf{C}, \mathbf{c}) = \prod_{i=1}^{10} \delta_i[C_i(t) - c_i]$. Derivatives of Π are

$$\frac{\partial \Pi}{\partial c_i} = \frac{\partial \delta_i}{\partial c_i} \prod_{\substack{n=1 \\ n\neq i}}^{10} \delta_n, \tag{18}$$

$$\frac{\partial \Pi}{\partial t} = -\sum_{i=1}^{10} \left[\frac{\partial \delta_i}{\partial c_i} \frac{\partial C_i}{\partial t} \prod_{\substack{n=1 \\ n\neq i}}^{10} \delta_n \right]. \tag{19}$$

Substitution of Eq. (18) into Eq. (19) yields

$$\frac{\partial \Pi}{\partial t} = -\sum_{i=1}^{10} \frac{\partial C_i}{\partial t} \frac{\partial \Pi}{\partial c_i}. \tag{20}$$

Multiplying the ith equation in Eqs. (1) with $\partial\Pi/\partial c_i$; applying the sifting property of the Dirac delta function, $g(x)\delta(x-y) = g(y)\delta(x-y)$; summing up the resulting ten equations (over $i = 1, \cdots, 10$); and accounting for Eq. (20) yields Eq. (14).

The initial condition (15) is obtained from its counterparts in Eq. (2).

Appendix B. Numerics for raw PDF equation

To solve Eq. (14) with the method of characteristics, we first write it as

$$\frac{\partial \Pi}{\partial t} + \sum_{i=1}^{10} g_i(\mathbf{c}) \frac{\partial \Pi}{\partial c_i} = -\sum_{i=1}^{10} \frac{\partial g_i}{\partial c_i} \Pi. \tag{21}$$

Then, a family of characteristics is defined by

$$\frac{\mathrm{d}c_i}{\mathrm{d}t} = g_i(\mathbf{c}), \quad i = 1, \cdots, 10. \tag{22a}$$

Along these characteristics,

$$\frac{\mathrm{d}\Pi}{\mathrm{d}t} = -\sum_{i}^{10} \frac{\partial g_i}{\partial c_i} \Pi. \tag{22b}$$

This equation is subject to the initial condition (15), which implies that the Dirac delta function from the initial state propagates along the characteristics unchanged. Numerical treatment requires an approximation of the delta function, e.g., as

$$\delta(x-y) \approx s_\Delta(x-y) = \frac{1}{\sqrt{2\pi\,\Delta^2}} \mathrm{e}^{-\frac{(x-y)^2}{2\Delta^2}}, \tag{23}$$

such that $s_\Delta(x-y) \to \delta(x-y)$ as $\Delta \to 0$. With this approximation, the initial condition (15) is replaced with

$$S_\Delta(\mathbf{c},0) = \left(\frac{1}{2\pi\Delta^2}\right)^5 \exp\left[-\frac{(C_{\text{tot}}-c_1)^2}{2\Delta^2} - \sum_{i=2}^{10}\frac{c_i^2}{2\Delta^2}\right] \tag{24}$$

and $\Pi(\mathbf{c},t) \approx S_\Delta(\mathbf{c},t)$ with $S_\Delta(\mathbf{c},t) \to \Pi(\mathbf{c},t)$ as $\Delta \to 0$.

For an nth MC realization of the random parameter set $\mathcal{A}_n$ ($n = 1, \cdots, N$), Eqs. (22) and (24) are solved using a standard numerical ODE solver, such as the fourth- and fifth-order Runge-Kutta method implemented in the Matlab function ODE45, to obtain the nth realization of $S_\Delta(\mathbf{c},t)$ denoted by $S_\Delta^{(n)}(\mathbf{c},t)$. The joint PDF $f(\mathbf{c};t)$ is obtained by averaging N MCS realizations,

$$f(\mathbf{c};t) \approx \frac{1}{N}\sum_{n=1}^{N} S_\Delta^{(n)}(\mathbf{c};t). \tag{25}$$

The results presented in the text correspond to $\Delta = 0.2$. This value provides a balance between the approximation of the Dirac delta function and the computational cost, which increases dramatically as $\Delta \to 0$.

References

Alawadhi, A., Boso, F., Tartakovsky, D.M., 2018. Method of distributions for water hammer equations with uncertain parameters. Water Resour. Res. 54, 9398–9411.

Alberts, B., Johnson, A., Lewis, J., Morgan, D., Raff, M., Roberts, K., Walter, P., 2014. Molecular Biology of the Cell, 6th ed. Garland Science.

Arumugam, S., Petrášsek, Z., Schwille, P., 2014. MinCDE exploits the dynamic nature of FtsZ filaments for its spatial regulation. Proc. Natl. Acad. Sci. U.S.A. 111, 1192–1200.

Boso, F., Tartakovsky, D.M., 2016. The method of distributions for dispersive transport in porous media with uncertain hydraulic properties. Water Resour. Res. 52, 4700–4712.

Chen, Y., Bjornson, K., Redick, S.D., Erickson, H.P., 2005. A rapid fluorescence assay for FtsZ assembly indicates cooperative assembly with a dimer nucleus. Biophys. J. 88, 505–514.

Chen, Y., Erickson, H.P., 2005. Rapid in vitro assembly dynamics and subunit turnover of ftsz demonstrated by fluorescence resonance energy transfer. J. Biol. Chem. 280, 22549.

Chen, Y., Erickson, H.P., 2009. FtsZ filament dynamics at steady state: subunit exchange with and without nucleotide hydrolysis. Biochemistry 48, 6664–6673.

Dajkovic, A., Lan, G., Sun, S.X., Wirtz, D., Lutkenhaus, J., 2008. MinC spatially controls bacterial cytokinesis by antagonizing the scaffolding function of FtsZ. Curr. Biol. 18, 235–244.

Dow, C., Rodger, A., Roper, D.I., van den Berg, H.A., 2013. A model of membrane contraction predicting initiation and completion of bacterial cell division. Integr. Biol. 5, 778–795.

Du, S., Pichoff, S., Kruse, K.J.L., 2018. FtsZ filaments have the opposite kinetic polarity of microtubules. Proc. Natl. Acad. Sci. U.S.A. 115, 10768–10773.

Erickson, H.P., Anderson, D.E., Osawa, M., 2010. FtsZ in bacterial cytokinesis: cytoskeleton and force generator all in one. Microbiol. Mol. Biol. Rev. 74, 504–528.

Falzone, T.T., Lenz, M., Kovar, D.R., Gardel, M.L., 2012. Assembly kinetics determine the architecture of α-actin in crosslinked f-actin networks. Nat. Comm. 3, 266–272.

Higdon, D., Kennedy, M., Cavendish, J., Cafeo, J., Ryne, R., 2004. Combining field data and computer simulations for calibration and prediction. SIAM J. Sci. Comput. 26, 448–466.

Huecas, S., Llorca, O., Boskovic, J., Martín-Benito, J., Valpuesta, J., Andreu, J., 2008. Energetics and geometry of FtsZ polymers: nucleated self-assembly of single protofilaments. Biophys. J. 94, 1796–1806.

Kennedy, M.C., O'Hagan, A., 2011. Bayesian calibration of computer models. J. R. Statist. Soc. B 63, 425–464.

Koskinen, M., Hotulainen, P., 2014. Measuring F-actin properties in dendritic spines. Front. Neuroanat. 8.

Lan, G., Dajkovic, A., Wirtz, D., Sun, S.X., 2008. Polymerization and bundling kinetics of FtsZ filaments. Biophys. J. 95, 4045–4056.

Masuda, H., Tan, Q., Awano, N., Wu, K.P., Inouye, M., 2012. Yeeu enhances the bundling of cytoskeletal polymers of MreB and FtsZ, antagonizing the CbtA (YeeV) toxicity in escherichia coli. Mol. Microbiol. 84, 979–989.

Mateos-Gil, P., Paez, A., Hörger, I., Rivas, G., Vicente, M., Tarazona, P., Véle, M., 2012. Depolymerization dynamics of individual filaments of bacterial cytoskeletal protein ftsz. Proc. Natl. Acad. Sci. U.S.A. 109, 8133–8138.

Medeiros, N., Burnette, D., Forscher, P., 2006. Measuring F-actin properties in dendritic spines. Nat. Cell Biol. 8, 215–226.

Needleman, D., 2015. The material basis of life. Trends Cell Biol. 25, 713–716.

Romberg, L., Mitchison, T.J., 2004. Rate-limiting guanosine5′-triphosphate hydrolysis during nucleotide turnover by FtsZ, a prokaryotic tubulin homologue involved in bacterial cell division. Biochemistry 43, 282–288.

Romberg, L., Simon, M., Erickson, H., 2001. Polymerization of FtsZ, a bacterial homolog of tubulin is assembly cooperative? J. Biol. Chem. 115, 11743–11753.

Ruiz-Martinez, A., Bartol, T.M., Sejnowski, T.J., Tartakovsky, D.M., 2016. Efficient multiscale models of polymer assembly. Biophys. J. 111, 185–196.

Ruiz-Martinez, A., Bartol, T.M., Sejnowski, T.J., Tartakovsky, D.M., 2018. Efficient models of polymerization applied to FtsZ ring assembly in escherichia coli. Proc. Natl. Acad. Sci. U.S.A. 115, 201719391.

Surovtsev, I.V., Morgan, J.J., Lindahl, P.A., 2008. Kinetic modeling of the assembly, dynamic steady state, and contraction of the FtsZ ring in prokaryotic cytokinesis. PLoS Comput. Biol. 4. E1000102

Swanson, D., Wingreen, N.S., 2011. Active biopolymers confer fast reorganization kinetics. Phys. Rev. Lett. 107, 218103.

Tartakovsky, D.M., Broyda, S., 2011. PDF Equations for advective-reactive transport in heterogeneous porous media with uncertain properties. J. Contam. Hydrol. 120–121, 129–140.

Tartakovsky, D.M., Gremaud, P.A., 2015. Handbook of Uncertainty Quantification. Springer, pp. 763–783.

Venturi, D., Tartakovsky, D.M., Tartakovsky, A.M., Karniadakis, G.E., 2013. Exact PDF equations and closure approximations for advective-reactive transport. J. Comput. Phys. 243, 323–343.

Wang, P., Tartakovsky, A.M., Tartakovsky, D.M., 2013. Probability density function method for Langevin equations with colored noise. Phys. Rev. Lett. 110, 140602.

Wang, P., Tartakovsky, D.M., 2012. Uncertainty quantification in kinematic-wave models. J. Comput. Phys. 231, 7868–7880.

Wegner, A., 1976. Head to tail polymerization of actin. J. Mol. Biol. 108, 139–150.